Click Here for Full Article

Late summer changes in burning conditions in the boreal regions and their implications for NO$_x$ and CO emissions from boreal fires

K. Lapina,[1] R. E. Honrath,[1] R. C. Owen,[1] M. Val Martín,[1,2] E. J. Hyer,[3] and P. Fialho[4]

[1] Building emission inventories for the fires in boreal regions remains a challenging task with significant uncertainties in the methods used. In this work, we assess the impact of seasonal trends in fuel consumption and flaming/smoldering ratios on emissions of species dominated by flaming combustion (e.g., NO$_x$) and species dominated by smoldering combustion (e.g., CO). This is accomplished using measurements of CO and NO$_y$ at the free tropospheric Pico Mountain observatory in the central North Atlantic during the active boreal fire seasons of 2004 and 2005. ΔNO$_y$/ΔCO enhancement ratios in aged fire plumes had higher values in June-July (7.3×10^{-3} mol mol^{-1}) relative to the values in August-September (2.8×10^{-3} mol mol^{-1}), indicating that NO$_x$/CO emission ratios declined significantly as the fire season progressed. This is consistent with our understanding that an increased amount of fuel is consumed via smoldering combustion during late summer, as deeper burning of the drying organic soil layer occurs. A major growth in fuel consumption per unit area is also expected, due to deeper burning. Emissions of CO and NO$_x$ from North American boreal fires were estimated using the Boreal Wildland Fire Emissions Model, and their long-range transport to the sampling site was modeled using FLEXPART. These simulations were generally consistent with the observations, but the modeled seasonal decline in the ΔNO$_y$/ΔCO enhancement ratio was less than observed. Comparisons using alternative fire emission injection height scenarios suggest that plumes with the highest CO levels at the observatory were lofted well above the boundary layer, likely as a result of intense crown fires.

1. Introduction

[2] Research in recent years has shown that the impact of boreal fires on tropospheric CO background levels is significant [*Novelli et al.*, 2003; *Edwards et al.*, 2004]. Measurements in fire plumes and modeling studies have also confirmed boreal fires as an important source of ozone precursors [*Val Martín et al.*, 2006; *Pfister et al.*, 2006; *Real et al.*, 2007], resulting in significant impacts on midlatitude lower free troposphere (FT) background O$_3$ during summer [*Lapina et al.*, 2006]. Large boreal wildfires can significantly affect tropospheric composition even in populated areas thousands of miles away, where anthropogenic sources usually dominate air quality impacts [*Wotawa et al.*, 2001; *Sapkota et al.*, 2005; *Colarco et al.*, 2004; *DeBell et al.*, 2004; *Morris et al.*, 2006].

[3] Quantifying and modeling fire emissions is a challenging task, because of the large degree of variability in the types of fire and fuel [*Kasischke et al.*, 2005]. Burning in the boreal forests is typically separated into two components with significantly different fuel characteristics and associated combustion processes: burning of aboveground vegetation and burning of organic soil layers (the ground layer) [*French et al.*, 2004]. The ground layer is located on the top of mineral soil and is made of litter, lichen, moss and organic soils [*Kasischke et al.*, 2005]. The amount of ground layer carbon is twice the amount of aboveground carbon, on average [*French et al.*, 2004], and therefore ground layer carbon may be a major contributor to the total amount of carbon emissions released during fires. Ground layer emissions are especially difficult to quantify, as the fraction of soil layer consumed is one of the most uncertain parameters in fire modeling [*Kasischke and Bruhwiller*, 2002; *French et al.*, 2004]. For example, recent field studies that measured the depth of burning in Alaskan fires indicate

[1]Department of Civil and Environmental Engineering, Michigan Technological University, Houghton, Michigan, USA.

[2]Now at Division of Engineering and Applied Sciences, Harvard University, Cambridge, Massachusetts, USA.

[3]Marine Meteorology Division, Naval Research Laboratory, Monterey, California, USA.

[4]Climate, Meteorology and Global Change Center, Group of Chemistry and Physics of the Atmosphere, University of the Azores, Terra Chã, Portugal.

that current fire models significantly underestimate the degree of consumption of surface layer fuels [*French et al.*, 2007].

[4] Burning of peatlands (i.e., sparsely forested lowlands) is another major source of emissions from fires [*Duncan et al.*, 2003; *Turquety et al.*, 2007]. Peatlands occupy 15–20% of the area of North American boreal regions, and research in the recent years has shown that they are as susceptible to burning as are well-drained upland ecosystems [*Turetsky et al.*, 2004].

[5] While CO emissions are greatest during smoldering combustion, NO$_x$ (NO + NO$_2$), a limiting factor for O$_3$ production, is mainly produced during the flaming stage of burning [*Lobert et al.*, 1991]. Therefore the emission ratio of NO$_x$/CO is related to the relative amounts of flaming and smoldering combustion. Because the NO$_x$/CO ratio (currently highly uncertain) plays an important role in estimates of NO$_x$ emissions and therefore O$_3$ production [e.g., *McKeen et al.*, 2002; *Cook et al.*, 2007], understanding the processes affecting its magnitude in fire plumes is of primary importance.

[6] The extent of ground layer burning in boreal regions increases through the growing season. Early in the season, soil layers are still frozen or saturated, and only dry vegetation on the surface is susceptible to burning. However, by late summer deeper soil layers have dried out and become flammable [*Kasischke and Johnstone*, 2005; *Turetsky et al.*, 2004]. As burning of ground layers occurs mostly via smoldering combustion [*Miyanishi*, 2001], this change in fuel properties is expected to result in an increase in both total carbon consumption and the relative importance of smoldering combustion, relative to flaming combustion. In particular, the increase in ground layer burning during the late fire season is expected to drive down the overall emission ratio of NO$_x$/CO (while increasing the total emissions of CO and possibly NO$_x$).

[7] The aim of this work is to use measurements in boreal fire plumes downwind of the source fires to assess the magnitude of this effect. Following emission, NO$_x$ is converted to nitric acid (HNO$_3$), peroxyacetyl nitrate (PAN) and other members of the NO$_y$ (total reactive nitrogen oxides) family. We therefore use ΔNO$_y$/ΔCO enhancement ratios in aged boreal fire plumes sampled during summers of 2004 and 2005 at the Pico Mountain observatory in the central North Atlantic to constrain NO$_x$/CO emission ratios in the upwind fires. The Boreal Wildland Fire Emissions Model (BWEM) [*Kasischke et al.*, 2005], a current model of boreal fire emissions of CO and NO$_x$, is also applied, together with the FLEXPART transport model, to estimate emissions and determine their consistency with the observations.

2. Methods

[8] This section starts with the description of the Pico Mountain observatory and measurements used in this work. The estimation of CO and NO$_x$ fire emissions for the 2004 and 2005 fire seasons using BWEM is described in section 2.2, and use of the FLEXPART transport model to generate time series of CO and NO$_x$ fire tracers at the observatory is described in section 2.3. Identification of fire events and selection of background levels of CO and NO$_y$ are described in sections 2.4 and 2.5.

2.1. Pico Mountain Station and Measurements

[9] The Pico Mountain observatory is located on the summit caldera of Pico Mountain in the Azores Islands (Portugal) in the central North Atlantic Ocean (38.78°N, 28.67°W). The observatory is frequently impacted by air from high-latitude regions, often without downwind transport over anthropogenic source regions [*Honrath et al.*, 2004]. It is therefore well suited to study the outflow from North American and Siberian boreal wildfires. The observatory's altitude (2225 m) is well above the marine boundary layer (MBL) during summer [*Kleissl et al.*, 2007] and the impact of island pollution on measurements is negligible [*Kleissl et al.*, 2007; *Val Martín et al.*, 2006].

[10] CO was determined using a nondispersive infrared absorption instrument (a modified Thermo Environmental, Inc., Model 48C-TL), calibrated daily with standards referenced to the NOAA Global Monitoring Division standard [*Novelli et al.*, 2003]. CO data were recorded as 1-min averages, and were further averaged to obtain the 30-min averages used in this work. Additional details on the instrument and calibration methods are provided in the works of *Honrath et al.* [2004] and *Owen et al.* [2006].

[11] NO, NO$_2$ and NO$_y$ were determined by an automated NO$_{x,y}$ system developed at Michigan Technological University, using established techniques: NO detection by O$_3$ chemiluminescence, NO$_2$ by conversion to NO via ultraviolet photodissociation and NO$_y$ by Au-catalyzed reduction to NO in the presence of CO. Measurements were recorded as 30-s averages (NO and NO$_2$) and 20-s averages (NO$_y$) every 10 min, and were averaged to obtain the 30-min averages used here. A detailed description of the system can be found elsewhere [*Val Martín et al.*, 2006; M. Val Martín et al., Seasonal variation of nitrogen oxides in the central North Atlantic lower free troposphere, submitted to *Journal of Geophysical Research*, 2007].

[12] To ensure that NO$_y$ observations were representative of air in the surrounding FT, we have excluded from this analysis (1) all periods potentially affected by upslope flow of MBL air [*Kleissl et al.*, 2007]; (2) measurements made during low to calm winds (wind speed <2 m/s), to avoid including NO$_y$ observations with potential for HNO$_3$ to be removed on the mountain surface; and (3) measurements with high ambient variability, to avoid including nitrogen oxides resulting from volcanic emissions, sometimes observed at this site under near-calm conditions [*Val Martín et al.*, 2006]. For this purpose, periods with high ambient variability were defined as in the work of *Val Martín et al.* [2006].

2.2. Boreal Wildland Fire Emissions Model

[13] BWEM is a model specifically developed to calculate emissions from boreal fires in the high-latitude regions of the Northern Hemisphere. The main feature that distinguishes BWEM from other wildland fire emissions models is its explicit consideration of surface organic layer consumption, which is a major contributor to fire emissions in boreal regions.

[14] Emissions were estimated separately for burning of aboveground vegetation and burning of the surface organic layer. There is no peatland category, although the deeper surface organic material and lower aboveground biomass of peatlands are accounted for by the forest inventory and soil

carbon database used in the model [*Kasischke et al.*, 2005]. For aboveground vegetation, BWEM employs a standard bottom-up approach, in which emission factors of CO and other species are applied to the estimated fuel consumption. To estimate emissions from ground layer consumption, BWEM accounts for variation in the depth of burning according to the month of burning and fire type (surface or crown) and for variations in carbon density of the surface layer.

[15] The potential carbon emissions (i.e., carbon emissions released if burning takes place) from burning of aboveground vegetation, $C_{p\_a}(t)$, and of the ground layer, $C_{p\_g}(t)$, are calculated as follows:

$$C_{p\_a}(t) = B_a f_{c\_a} F_{b\_a} \beta_a(t) \tag{1}$$

and

$$C_{p\_g}(t) = \int_0^{d_b(t)} C_g(x) dx, \tag{2}$$

where B_a is aboveground carbon density, f_{c_a} represents the biomass carbon content ($f_{c\_a} = 0.45$), F_{b_a} is the biomass fraction available for burning, $\beta_a(t)$ is the fractional fuel consumption (a function of biomass density and fire type), $C_g(x)$ is the carbon density of the surface organic layer as a function of depth, x, and $d_b(t)$ is the depth of burning.

[16] Crown and surface fires are considered separately by the BWEM, and the prevalence of crown fires increases from 70% of area burned early in the fire season (before 1 June) to 90% of area burned after 1 August. Crown fires consume more aboveground vegetation (have high $\beta_a(t)$) and the depth of ground layer burning is also higher, because they typically burn in drier conditions compared to surface fires. The depth of burning was varied seasonally within BWEM by using different values of $d_b(t)$ for early (before 1 June), midseason (1 June to 31 July) and late (August and later) fires. Late season fires have values of $d_b(t)$ twice those of fires earlier in the season (1 June to 31 July). As a result of these assumptions, greater carbon emissions (i.e., emissions of CO$_2$, CO, hydrocarbons and carbonaceous particles) are generated by fires occurring later in the growing season [*Kasischke et al.*, 2005].

[17] In the BWEM as applied in this work, the ratio of flaming to smoldering was 80:20 for aboveground biomass and 20:80 for the surface organic layer. Potential emissions of other species can be obtained from potential carbon estimates using emission factors relative to total carbon as a function of combustion type: EF_f, for flaming, and EF_s, for smoldering. For CO, we used the BWEM emission factors: 460 and 190 g of CO per kilogram of carbon burned for smoldering and flaming, respectively [*Kasischke and Bruhwiller*, 2002]. For NO$_x$, emission factors were selected on the basis of a review of available literature, as described in section 2.2.2 below. Potential emissions were then combined with estimates of area burned using a geographic information system (GIS). Emissions of any species, $E(t)$, were obtained using:

$$E(t) = A(t) \{ EF_f [0.8 C_{p\_a}(t) + 0.2 C_{p\_g}(t)] + EF_s [0.2 C_{p\_a}(t) + 0.8 C_{p\_g}(t)] \}, \tag{3}$$

where $A(t)$ is the area burned. Early in the season (June–July) an overall smoldering/flaming ratio in the model is 1.3, on average, and later in the season it is 2.0, as the prevalence of smoldering increases because of higher levels of fuel consumption in surface organic layers. This results in enhanced emissions (per unit fuel combusted) of compounds with larger emission factors for smoldering combustion (e.g., CO and hydrocarbons) and reduced emissions (per unit fuel combusted) of flaming combustion products (e.g., NO$_x$). NO$_x$/CO emission ratios drop correspondingly (see section 3.2).

[18] Burned area and fire locations for Alaska were obtained from the Alaska Fire Service [*Kasischke et al.*, 2002]. For Canada, burned area was obtained from the Canadian Forest Service (http://cfs.nrcan.gc.ca/regions/nofc). Because these data were available at the provincial level only, fire locations were determined from MODIS hot spots. Information on the temporal distribution of the fires in both regions was obtained from MODIS hot spot data. Despite incomplete information due to satellite coverage limitations, this approach has been shown to adequately represent day-to-day variability in emissions time series for atmospheric modeling applications [*Hyer et al.*, 2007a; *Roy et al.*, 2007].

[19] Emissions were calculated on a 1° × 1° grid, on a daily basis and assuming typical burning conditions (moderate severity scenario) [*Kasischke et al.*, 2005]. A more detailed description of the model can be found in the work of *Kasischke et al.* [2005].

2.2.1. Fires in Siberia

[20] The emissions simulated by BWEM and used in this work include North American emissions only. Large areas burn every year in Siberia (approximately three times those in North America, on average [*Soja et al.*, 2007]). Although Siberian fire emissions can impact the Pico Mountain measurement site [*Honrath et al.*, 2004; *Lapina et al.*, 2006], such impacts have been reported during exceptionally large fire years (i.e., 2003). The impact of Siberian emissions at the Pico Mountain station during 2004 is expected to be small relative to the North American fires, as 2004 was a low-fire year in Siberia. 2005 was a relatively high-fire year for Siberia [*Soja et al.*, 2007]. Therefore, it is possible that some impact of Siberian emissions was present during the summer 2005. However, during time periods affected by fires from both source regions, we expect the impact of North American fires to be larger because of their relative proximity to the observatory. Hence, the fire periods discussed below, selected on the basis of North American fire impacts, are expected to be characteristic of North American fires.

2.2.2. NO$_x$ Emission Factors

[21] Daily NO$_x$ fire emissions were obtained using equation (3), which requires knowledge of NO$_x$ emission factors. NO$_x$ is a flaming stage compound [*Lobert et al.*, 1991] and is produced in smaller amounts during smoldering combustion, as laboratory studies have shown [*Yokelson et al.*, 1997]. The combustion temperatures in biomass fires are insufficient for significant conversion of atmospheric N$_2$ to NO$_x$ [*Andreae*, 2004]. Hence, NO$_x$ emissions reflect the nitrogen content of the fuel, which is considered to be relatively low in boreal vegetation [*Wofsy et al.*, 1992]. This, and the fact that a large fraction of biomass in the

boreal fires is consumed via smoldering combustion, result in lower NO$_x$ emission factors for boreal fires compared to fires in other regions. However, currently there are few field observations of NO$_x$ from boreal fires available, and the existing emission factors exhibit large variability, making the modeling of NO$_x$ emissions a challenging task.

[22] *Goode et al.* [2000] performed field measurements of NO$_x$ emission factors from boreal wildfires in Alaska. They reported an average emission factor (which includes fire observations made by *Nance et al.* [1993]) of 1.54 g NO$_x$ as NO per kilogram fuel burned. In the units reported in this work this corresponds to 3.42 g NO$_x$ as NO per kilogram carbon burned. The measured fires were predominantly flaming crown and surface fires, and emission factors for predominantly smoldering fires, such as peat fires, are expected to be lower.

[23] While many studies use a single NO$_x$ emission factor that incorporates both smoldering and flaming combustion processes [*Andreae and Merlet*, 2001], we took advantage of BWEM's ability to allocate emissions by combustion type. To obtain emission factors for the flaming and smoldering stages of combustion, we referred to laboratory measurements, reported by *Yokelson et al.* [1996], because the field studies report only fire-integrated estimates. We chose the emission factors for smoldering and flaming combustion obtained for fuel described as "broadcast" by *Yokelson et al.* [1996], 0.0656 NO and 0.0189 NO$_2$ for flaming combustion and 0.0167 NO and 0.0019 NO$_2$ for smoldering combustion, in units of moles per kilogram fuel. These correspond to EF$_f$ = 5.64 and EF$_s$ = 1.24 (g NO$_x$ as NO per kilogram carbon) for flaming and smoldering combustion, respectively. The broadcast fuel was made up of a mixture of decomposing organic matter, pine needles, twigs, and wood. To test whether the selected values of EF_f and EF_s are reasonable, we input them into BWEM under the average fuel consumption scenario to derive fire-integrated emission factors. The derived estimates were in a good agreement (within 25%) with the field observations [*Goode et al.*, 2000].

[24] On the basis of the selected emission factors, the NO$_x$/CO emission ratio for purely smoldering combustion in the model was 3×10^{-3} mol mol^{-1}, while the emission ratio for purely flaming combustion was 28×10^{-3} mol mol^{-1}. This results in NO$_x$/CO emission ratios of 18×10^{-3} mol mol^{-1} for aboveground vegetation and 5×10^{-3} mol mol^{-1} for the surface organic layer.

2.3. FLEXPART Simulations

[25] The Lagrangian particle dispersion model FLEXPART [*Stohl et al.*, 2005] was used to calculate mixing ratios of CO and NO$_x$ tracers at the Pico Mountain observatory resulting from the BWEM-estimated fire emissions, to assess the potential impact of wet deposition on nitrogen oxides levels in the fire plumes and to evaluate emissions injection height scenarios. FLEXPART (version 6.2) was driven with data from the European Centre for Medium Range Weather Forecasts (ECMWF) [*European Centre for Medium-Range Weather Forecasts*, 2005] with a $1° \times 1°$ horizontal resolution, 61 vertical levels and a temporal resolution of 3 h, using meteorological analysis at 0000, 0600, 1200, and 1800 UTC, and ECMWF 3-h forecasts at intermediate times (0300, 0900, 1500, 2100 UTC).

[26] Forward FLEXPART runs were used to simulate the advection and dispersion of fire emissions tracers. These results were used to analyze the vertical distribution of emissions. Particles representing fire emissions were released over 3-h intervals above the locations of active fires, at altitudes determined by the height scenarios (see section 2.3.1). The number of particles released into each grid cell was scaled by the mass of emissions in each grid cell. Particles were dropped from the simulation after 20 days and were conserved up to that time. Thus, the simulations model only enhancements caused by fire emissions over the previous 20 days.

[27] Backward FLEXPART simulations (i.e., retroplumes) were used to calculate mixing ratios of fire tracers at the measurement site and to determine the transport pathways of air before arriving at the observatory. Retroplumes were initiated every 3 h using 4,000 particles released over a 1-h time interval into a $1° \times 1°$ grid box centered on the observatory, over an altitude range of 2000–2500 m asl. Particles were followed backward in time for 20 days. In order to account for differences in air density between the release cell and upwind sources, the upwind residence times of the particles were normalized by the local air density. Normalized particle residence times were convolved with North American boreal fire CO emissions (section 2.2) according to the technique described by *Seibert and Frank* [2004] to obtain CO fire tracer mixing ratios at the Pico Mountain station, CO$_{BB_T}$. Emissions were convolved with the retroplumes from the surface layer up to the maximum injection height of emissions. The same approach was employed to obtain simulations of NO$_{xBB_T}$, an inert tracer representing NO$_x$ fire emissions. Since particles are tagged with their release times, the travel time of air sampled at the observatory can be estimated.

[28] To identify periods when anthropogenic impacts were significant (in order to omit these periods from the analyses presented below), we performed FLEXPART simulations of anthropogenic tracers. Anthropogenic tracers representing North American, European, and Asian emissions, were obtained in a manner similar to the fire tracers, except that emissions were convolved with the retroplumes in the footprint layer only (0–300 m). All three sources had significant impacts, although North American emissions were dominant. Anthropogenic emissions were based on the EDGAR 3.2 Fast Track 2000 data set [*Olivier and Berdowski*, 2001] with 1° resolution.

2.3.1. Injection Height of Fire Emissions

[29] The injection height plays an important role in the fate of fire emissions, as it influences their long-range transport and lifetime. It is affected by numerous factors, which include not only fire characteristics (e.g., intensity and type) but also meteorological conditions present at the time of burning [*Trentmann et al.*, 2006; *Luderer et al.*, 2006].

[30] Because of this complex behavior, we selected an arbitrary scenario, consistent with our understanding of processes that affect fire injection height in the boreal regions. In this scenario, emissions were released between the surface and 7.5 km with a constant mixing ratio throughout the column. This choice is consistent with limited field observations and was based on the results of other recent boreal fire modeling studies, most of which have distributed emissions with constant mixing ratio

between the surface and a selected maximum height [*Damoah et al.*, 2006; *Pfister et al.*, 2005; *Stohl et al.*, 2006; *Cook et al.*, 2007]. For example, *Cook et al.* [2007] distributed emissions from surface up to 10 km, while *Stohl et al.* [2006] injected emissions into the lowest 3 km of the model atmosphere. *Hyer et al.* [2007a] found that emissions injected by constant mixing ratio through the tropospheric column or injected into the midtroposhere ($\sim$500 hPa) resulted in the best agreement with MOPITT observations. An alternative approach is to distribute emissions within selected layers of the modeled atmosphere to account for significant contributions from a particular fire type. For example, to simulate large contributions from peat fires, *Turquety et al.* [2007] released 40% of the emissions into the boundary layer (with the remaining 60% evenly divided between the middle and upper troposphere), while *Generoso et al.* [2007] implemented a scheme in which the fraction of total emissions increased with height up to a maximum level (which varied from 3 to 6.5 km), similar to the impact of convection generated by intense crown fires. *Turquety et al.* [2007] performed a sensitivity study of chemical transport model simulations of the 2004 North American fires, which showed that at least half of the emissions needed to be injected above the model boundary layer to match MOPITT CO data. By choosing a maximum injection height of 7.5 km, we place a major fraction of emissions (about 70%) above the boundary layer.

[31] The 2004 North American fires were also studied by *Mazzoni et al.* [2007] who determined the injection heights of individual fire plumes using satellite data and found somewhat lower numbers, with a maximum height of 5.2 km and a mean of 2.4 km. However, these results may be biased by inherent limitations of the spaceborne sensor, including exclusion of cloudy pixels and undersampling due to the infrequent overpasses. For example, no pyroconvective events lofting emissions to the upper troposphere or lower stratosphere [*Fromm and Servranckx*, 2003; *Jost et al.*, 2004; *Fromm et al.*, 2005] were observed, while such occurrences were documented in 2004 [*Damoah et al.*, 2006].

[32] For comparison purposes, an additional run in which all emissions were injected into the lowest layer of the model (0–300 m) was also conducted. In all cases the model was run with the FLEXPART convective scheme turned on. Previous work has demonstrated the effectiveness of this scheme to transport emissions as high as the stratosphere for specific extreme events, even when a relatively low initial injection height (3 km) was used [*Damoah et al.*, 2006]. As will be discussed below (section 3.4), the comparison between these two runs showed that simulations employing a 7.5 km maximum injection height best reproduced the observations at the Pico Mountain observatory, indicating the importance of placing a significant fraction of emissions above the boundary layer. The higher release height also resulted in faster model transport and reduced wet removal (section 2.3.2). However, the choice of injection height was not critical for the conclusions presented below, as the choice of fire periods and modeled NO$_x$ to CO enhancement ratios did not significantly change when the 300 m injection height simulations were used instead.

2.3.2. Assessment of Wet Removal

[33] To compare the fire-affected periods in terms of the amount of precipitation during transport to the Pico Moun-tain observatory, which may have affected NO$_y$ levels, we performed a "wet" run, in which NO$_{xBB_T}$ underwent wet removal in the model. As the emphasis was on a plume-to-plume comparison, rather than accurate modeling of NO$_y$ deposition, and since interconversion among NO$_y$ species is not modeled in FLEXPART, a simplified method was employed.

[34] FLEXPART allows the choice of species and their first-order physicochemical parameters in the modeling of wet deposition, which takes the form of an exponential decay process during precipitation [*Stohl et al.*, 2005]. We applied the default NO$_2$ wet scavenging parameters, provided in FLEXPART, to all NO$_y$ in the model, and computed removal that would have occurred if all NO$_y$ were scavenged as is NO$_2$. These simulations are defined as NO$_{xBB_w}$. NO$_2$ was chosen because of its moderate removal efficiency. The results are presented below in terms of f_{WET}, the fraction of NO$_x$ tracer removed in the wet run, relative to the NO$_{xBB_T}$ (inert tracer) simulation (i.e., (NO$_{xBB_T}$−NO$_{xBB_w}$)/NO$_{xBB_T}$). While f_{WET} is not meant to be an accurate estimate of wet deposition of NO$_y$ in the fire plumes, the calculated values are instructive as an indication of the relative importance of precipitation among the events analyzed.

[35] Runs performed using 300 m and 7.5 km release heights showed similar event-to-event differences, although the lower release height resulted in higher NO$_{xBB_T}$ removed (f_{WET} in the range of 0.45–0.85, with the mean value of 0.55, compared to the range of 0.26–0.70 and the mean value of 0.41 for the base run). This higher removal was a result of the longer residence time of emissions in the boundary layer during transport to Pico. Also, as no wet removal was assumed to occur in the initial step when emissions were injected up to 7.5 km, f_{WET} in this run can be underestimated if there were precipitation in the fire cloud.

2.4. Fire-Affected Events Selection

[36] Fire-affected time periods were identified on the basis of high CO observations and enhanced FLEXPART CO fire tracer. CO was considered to be high when the 30-min average mixing ratio exceeded the estimated boreal CO background (section 2.5) by at least 5 ppbv. For a high-CO period to be considered a fire-affected event, the presence of fire emissions had to be confirmed by elevated CO$_{BB_T}$ mixing ratios and CO$_{BB_T}$ had to exceed anthropogenic CO tracers during the event period or within ± 6 h. In this way we limited our analysis to periods affected predominantly by fire emissions. We excluded periods when high relative humidity (above 96%) was observed at the observatory, as such conditions favor removal of the nitric acid component of NO$_y$ thus potentially biasing the ΔNO$_y$/ΔCO analysis.

[37] When averaging model results for the fire-affected periods, the start and end of each event were adjusted by up to ±6 h relative to the original start and end of the event, in order to maximize the average CO$_{BB_T}$ over the period of same length. This was done in order to account for errors in transport modeling, e.g., periods when the model simulated an event a few hours earlier or later than it occurred in reality.

2.5. Estimation of Background Levels and Enhancement Ratios

[38] Enhancement ratios of NO$_y$ for the fire-affected periods are presented below (section 3.5). Enhancement

ratios of NO$_y$ (ΔNO$_y$/ΔCO) were calculated by averaging ΔNO$_y$ and ΔCO for each period and taking their ratios, where ΔNO$_y$ and ΔCO are defined as enhancements over the background levels of these species. Enhancement ratios depend critically on the background values used. Therefore, the remainder of this section discusses the estimation of the background levels for the fire-affected periods.

[39] To estimate the CO background values in the boreal fire plumes, we averaged CO monthly observations at two boreal stations, Alert and Barrow. These CO measurements are made by the NOAA Earth System Research Laboratory, Global Monitoring Division (available at http://www.esrl. noaa.gov/gmd), and are screened for nonbackground values. We obtained daily varying CO boreal backgrounds by linearly interpolating between the monthly values. Responding to a seasonal change in OH concentrations, CO background levels drop sharply from June to July and then increase slowly in the late summer. Since this seasonal process continues to affect air during its transport to the Pico Mountain observatory, the effective CO boreal background is different from the one when the air mass left the source region (approximately 10 days prior, on average). To account for this change, we used boreal background values corresponding to the day the measurements were made. CO background values obtained in this way ranged from 87 to 97 ppbv for the studied time periods, with the mean of 92 ppbv.

[40] To assess whether these background values are reasonable, we compared them to CO mixing ratios observed during boreal outflow in the absence of fires. We identified three such periods prior to the start of large fires: 0500–0900 UTC 7 June 2004, 0800–1900 UTC 19 June 2004, and 0530–1200 UTC 31 May 2005. Model simulations indicated near-zero fire impact during these times. The difference between the estimated background levels and the mean observed CO mixing ratios in boreal outflow without the presence of fire emissions was not significant, less than 8 ppbv. This estimation may be an upper limit on the potential bias of the background calculation as this comparison was obtained during the late spring/early summer season when ambient CO levels undergo fast transition due to a sharp rise in OH levels.

[41] For the NO$_y$ background, we used the mean mixing ratio observed at the Pico Mountain station during the same periods (except the period on 19 June, when NO$_y$ measurements were unavailable). The resulting NO$_y$ background mixing ratios were 139 ppbv for 2004 and 214 ppbv for 2005. These mixing ratios were close to the lowest values observed during the fire-affected periods. During most events, ΔNO$_y$ was only weakly sensitive to uncertainty in these background values, since NO$_y$ enhancements in the fire plumes were usually large. For example, a 25% change in the presumed NO$_y$ backgrounds would result in a 13% change of ΔNO$_y$ on average, and would not significantly affect the results presented below.

3. Results and Discussion

[42] We start this section with the discussion of the generated CO fire inventory and its comparison to other existing inventories. Next, simulated fire NO$_x$/CO emission ratios are discussed in the context of measurements and modeling studies (section 3.2). Fire tracers at the Pico

Mountain station are compared with observations during the fire-affected periods for two injection height scenarios in sections 3.3 and 3.4. Finally, the variability in observed ΔNO$_y$/ΔCO enhancement ratios is used to assess the presence of seasonality in NO$_x$/CO emission ratios from fires.

3.1. BWEM CO Emissions Estimates

[43] Figures 1a and 1b present the calculated daily emissions of CO from boreal fires in North America for the summers of 2004 and 2005. These seasons were the largest and third-largest on record in Alaska, respectively (Center for International Disaster Information, http:// www.cidi.org/wildfire). Large areas were also burned in Canada (National Forestry Database Program, http:// nfdp.ccfm.org/compendium/fires), thus making 2004 and 2005 large fire years in boreal North America [*Pfister et al.*, 2005; *Stohl et al.*, 2006; *Turquety et al.*, 2007; *Soja et al.*, 2007]. Here we compare our CO inventory for Alaskan and Canadian wildfires with other existing inventories, and discuss the reasons for observed differences.

[44] Two other independent CO emission inventories were developed for the 2004 North American boreal fire season. *Pfister et al.* [2005] used an inverse modeling approach to constrain 2004 fire CO emissions using MOPITT observations and MOZART chemical transport model simulations. They applied a weekly adjustment to their a priori emissions estimate, which resulted in more than a twofold increase in the total summer emissions. Another inventory for the 2004 fires was developed by *Turquety et al.* [2007], who used a bottom-up approach with emphasis on the large deduced contribution of peat burning. Although these approaches differed, both inventories resulted in an estimate of 30 Tg CO released from Alaskan and Canadian fires over 2004 summer season, with *Pfister et al.* [2005] reporting an uncertainty of ±5 Tg CO. We obtained a somewhat higher estimate of 37 Tg CO using BWEM. (For comparison, anthropogenic CO emissions for the entire continental U.S. during the same period were approximately 25 Tg CO [*Pfister et al.*, 2005].) In addition, there are significant differences in the timing of these emissions. For example, while all three inventories predict large peaks in CO emissions at the end of June and throughout July, BWEM emissions stay high throughout August (Figure 1a). A decrease in burned area in August resulted in the decline in emissions in the previous inventories, while the higher August emissions in BWEM are the result of accounting for deeper burning of the organic soil layer in late summer.

[45] *Turquety et al.* [2007] introduced a linearly increasing daily scaling factor (ranging from 0.67 on 1 June to 1.33 on 31 August) to account for an increase in peat fuel consumption due to drying as summer progressed. However, no such increase was applied to the burning of surface organic layer in the upland forests. Consequently, their late season estimates are likely too low. *Pfister et al.* [2005] noticed that their adjustment to the a priori emissions increased as summertime advanced. They suggested a further thawing of surface layers and intensifying peat fires as a possible explanation for this increase. However, their a posteriori August CO emissions were still significantly lower (by 11 Tg) than the BWEM-estimated emissions for
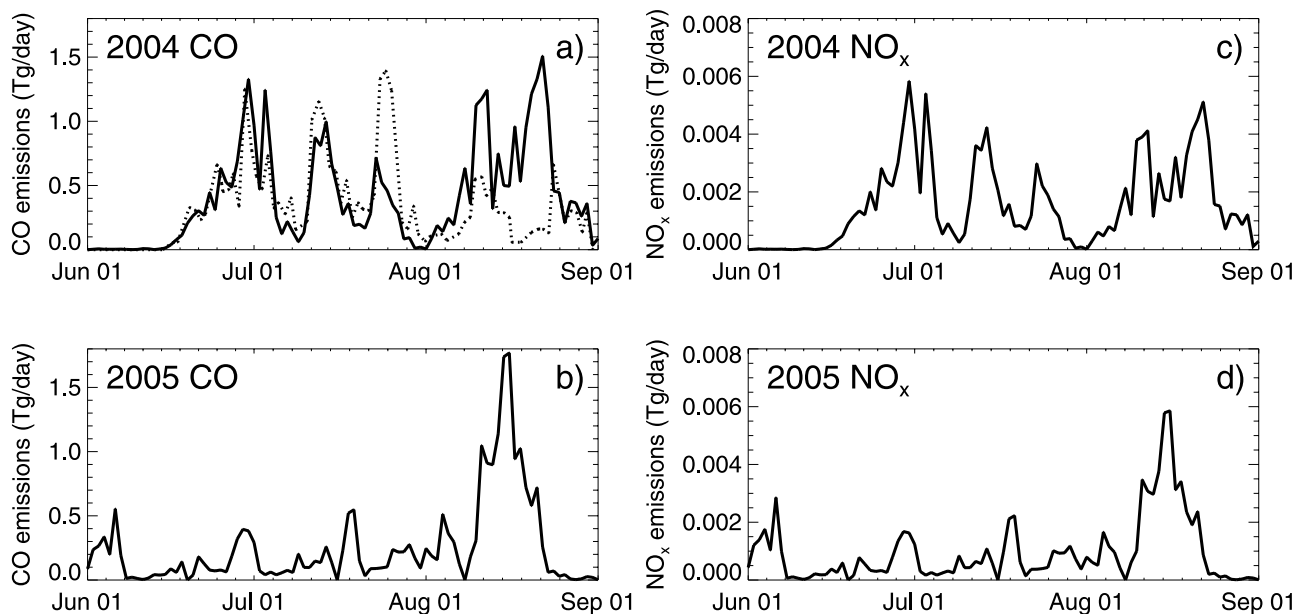
Figure 1. Estimated emissions from North American boreal fires during the summers of 2004 and 2005, derived with BWEM (solid lines) for (a and b) CO (in units of Tg d^{-1}) and (c and d) NO$_x$ (in units of Tg N d^{-1}). The prior CO emissions estimate of *Pfister et al.* [2005] is plotted for comparison (dotted line in Figure 1a).

the same time period. To further investigate this difference, we used FLEXPART simulations (section 2.3) of the vertical distribution of fire emissions over the region and time period used for inversion by *Pfister et al.* [2005]. On average, 30% of the CO mass in the studied region was present below 2 km, where MOPITT's sensitivity is low. This number increased to more than 50% for the run with emissions injected within the lowest 300 m. Provided a late season increase in smoldering emissions is associated with much of emissions to be released near the ground, this change may therefore have contributed to an underestimation of total CO by the MOPITT-based inversion. (For a discussion of the effects of MOPITT vertical sensitivity on estimated source magnitudes, see the work of *Hyer et al.* [2007b]). However, smoldering emissions, the production of which is expected to increase in the late summer, do not necessarily originate from the low-intensity ground fires, typically characterized by low injection height, but they can be a result of more frequent high-energy crown fires in the late season [*Kasischke et al.*, 2005]. Therefore, although changes in the injection height of emissions are possible, there is not enough information available at present to draw conclusions regarding the nature of these changes.

[46] A more detailed intercomparison of CO inventories, which would account for differences in methodologies (including, for example, the fact that each inventory used different sources for burned areas) is beyond the scope of this work. Current methods used for building fire emission inventories have very large uncertainties, making it challenging to find the best estimate.

[47] We are not aware of any other existing inventories for 2005 boreal fire season available for comparison with this work. Fire activity in North American boreal regions during 2005 was lower than in 2004, and we derived 23.5 Tg CO for the total summer 2005 emissions.

3.2. NO$_x$ Emissions and NO$_x$/CO Emission Ratios

[48] We estimated total NO$_x$ emitted from the North American boreal fires during the summers of 2004 (Figure 1c) and 2005 (Figure 1d) as 0.145 Tg N and 0.088 Tg N, respectively.

[49] Daily fire NO$_x$/CO emission ratios were calculated by dividing total NO$_x$ fire emissions by total CO fire emissions for that day. Emission ratios depend on multiple model parameters, which include the depth of burning, allocation of flaming/smoldering, and choice of emission factors for CO and NO$_x$. The average emission ratio dropped from 9×10^{-3} mol mol^{-1} in June and July to 7×10^{-3} mol mol^{-1} in August, with the summer average of 8×10^{-3} mol mol^{-1}, for both 2004 and 2005. The drop in the emission ratio in August is a result of the increase in the amount of organic soil layer consumed later in the burning season, as described above (section 2.2).

[50] Although previous boreal fire emission inventories have not considered a seasonal decline in NO$_x$/CO emission ratios, their ratios are in general agreement with the BWEM seasonal average value. For example, *Cook et al.* [2007] selected 8×10^{-3} mol mol^{-1} as the optimal NO$_x$/CO emission ratio for their model to best match the aircraft and satellite observations of the 2004 Alaskan and Canadian fire plumes in July. *McKeen et al.* [2002] reported ΔNO$_y$/ΔCO observations of 7×10^{-3} mol mol^{-1} in late June in North American fire plumes less than 50 h old and used this number as a reasonable fit for the emission ratio in their model simulations. Observations of fresh (less than 1 day old) Alaskan fire plumes by *Wofsy et al.* [1992] give a lower value, 5.6×10^{-3} mol mol^{-1}, which the authors suggested may have indicated smoldering tundra fires as the source. *Goode et al.* [2000] sampled air over the Alaskan fires in the late June and measured NO$_x$/CO ratio of 18×10^{-3} mol mol^{-1}. The same value was obtained by *Wofsy et al.* [1994]
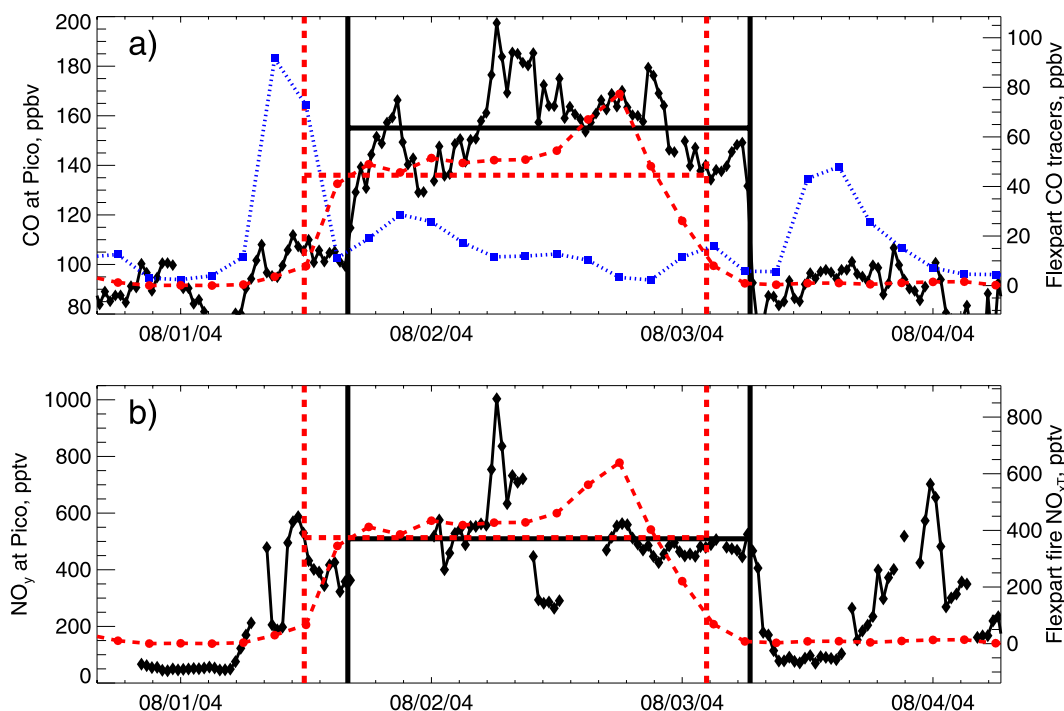
Figure 2. Comparison of measurements with modeled fire tracers during the fire event on 1–3 August 2004, for (a) CO and (b) NO$_y$. Measurements (black), modeled fire tracer (dashed line), and North American anthropogenic CO tracer (dotted line in Figure 2a) are shown. Horizontal lines show the average values for the event. Vertical lines indicate the beginning and end of the actual event (solid lines) and of the period corresponding to the modeled event in the FLEXPART (dashed lines). The right axis is offset so that zero tracer mixing ratio is aligned with the estimated boreal background.

who sampled fire-affected air masses in NE Canada from the middle to late July. These high numbers were likely the result of predominantly flaming nature of sampled fires.

3.3. Fire-Affected Periods and Comparison of Model to Observations

[51] Twelve fire-affected periods satisfying the criteria described in section 2.4 were identified: seven events in 2004 and five events in 2005 (see Table S1 in the auxiliary material[1] for the start and end times of the events). NO$_y$ levels were significantly enhanced in all selected periods. (The 2004 periods selected here are nearly identical to those previously identified by *Val Martín et al.* [2006].)

[52] The majority of the fire plumes observed at the Pico Mountain station have a finely detailed structure, characterized by short-term variability in CO and NO$_y$ that is typically not reproduced by the FLEXPART simulations. An example of this is shown in Figure 2. (For additional examples of measurements obtained during the fire-affected periods and time periods in the absence of fire emissions, see *Val Martín et al.* [2006, Figures 1 and 3].) However, averaging over the events' duration leads to a reasonably good agreement between the observations and simulated tracers. Scatterplots of the mean FLEXPART tracer mixing ratios for each event versus the event mean CO and NO$_y$ enhancements are shown in Figure 3. FLEXPART generally

captured the timing and relative magnitudes of the fire events ($r = 0.76$ and $r = 0.89$ for CO and NO$_y$, respectively). The better correlation for NO$_y$ was likely the result of reduced sensitivity to variability in the background, as discussed in section 2.5.

[53] The regression slopes are 1.1 for CO and 1.3 for NO$_y$. The slopes were calculated using the geometric mean (reduced major axis) two-sided regression technique [*Ayers*, 2001; *Draper and Smith*, 1998]. To use these slopes to evaluate the consistency of the measurements with the BWEM emissions, it is necessary to consider the fact that losses during transport to the station are possible. For CO, loss of less than 20% by reaction with OH is expected over the 7–15 day transport period, if OH concentrations in the fire plumes are low as was concluded by *de Gouw et al.* [2006] ([OH] = 4.5×10^5 cm^{-3}). This would produce a tracer/observed enhancement slope of ≤ 1.25, if the emissions inventory and transport model were accurate. The regression slope of 1.1 thus indicates rather good agreement.

[54] For NO$_y$, significant removal is expected, mainly via wet scavenging of HNO$_3$ and therefore a slope significantly greater than unity is expected. For anthropogenic emissions, a majority of NO$_y$ (>80%) is typically lost before or during transport out of the boundary layer [*Stohl et al.*, 2002; *Parrish et al.*, 2004; *Li et al.*, 2004; *Hudman et al.*, 2007]. The fraction of NO$_y$ from the fires that is lost may be significantly lower, however, for several reasons [*Val Martín et al.*, 2006]. First, PAN/HNO$_3$ ratios in boreal fire

---
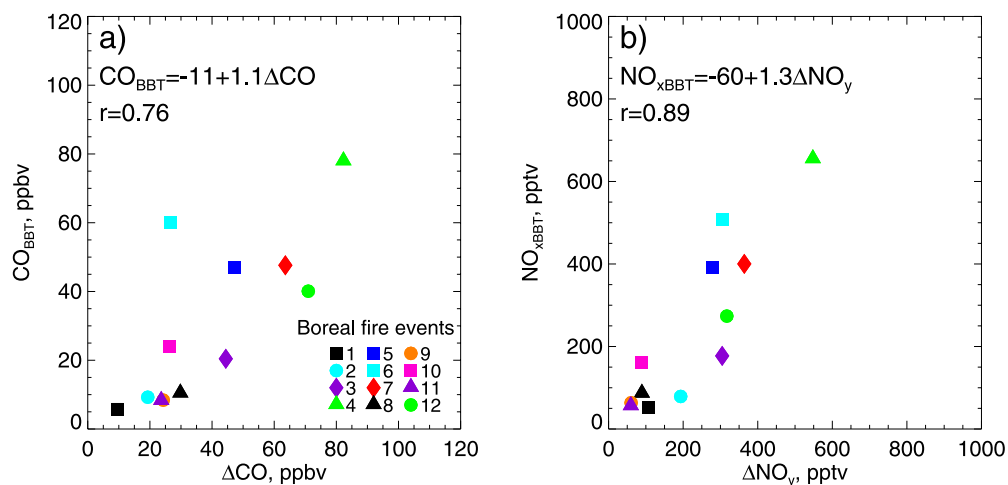
Figure 3. Scatterplot of simulated tracer mixing ratios against observed enhancements, averaged over each event: (a) CO$_{BB_T}$ versus ΔCO and (b) NO$_{xBB_T}$ versus ΔNO$_y$. Fire events (Table S1 in the auxiliary material) are coded as shown in the legend.

plumes are larger than those in typical anthropogenic source regions, because of lower NO$_x$/NMHC emission ratios and cooler temperatures [*Jacob et al.*, 1992; *Mauzerall et al.*, 1998; *Mason et al.*, 2001]. For example, the airborne measurements of the North American fire plumes over the eastern U.S. determined that more than half of the NO$_y$ in the plumes was in the form of PAN. Nitric acid and aerosol nitrate were also significantly elevated, while NO$_x$ concentrations were low [*Singh et al.*, 2007]. Since PAN is not effectively removed by wet deposition, this is expected to increase NO$_y$ transport efficiency. Second, rapid convection associated with large fires may result in relatively ineffective removal of soluble species; for example, relatively significant amounts of black carbon particles can survive such uplift [*Stohl et al.*, 2006]. Third, convection-induced injection into the cold FT leads to a long lifetime for PAN, which can then be transported long distances [*Singh et al.*, 2007; *Cook et al.*, 2007]. Finally, dry conditions during transport in the FT can also lead to inefficient removal of nitric acid.

[55] Since the magnitude of NO$_y$ loss during lofting and transport to the Pico Mountain station is not known, it is not possible to quantitatively evaluate the NO$_y$ regression slope. The slope of 1.3 is consistent with ~25% loss, and suggests that either NO$_y$ loss was low and of that approximate magnitude, or loss was greater but NO$_x$ emissions were underestimated.

3.4. Impact of Emission Injection Height

[56] To determine the sensitivity of the simulations to the emissions injection height, we compared the standard FLEXPART simulation results to those from the run in which all emissions were released within the lowest 300 m layer. The correlation of the resulting tracer simulations was significantly worse than in the base run (Figure 3): the correlation coefficient dropped by more than 30% for both species and the regression slopes dropped by nearly 40%. Hence, use of the low maximum release height resulted in underestimation of mixing ratios at the Pico Mountain station. While this comparison to the Pico Mountain obser-

vations alone is insufficient to constrain the magnitude and injection height of all emissions [*Leung et al.*, 2007], these results support the conclusions of previous research that releasing emissions above the boundary layer is important for adequate modeling of boreal fires [*Turquety et al.*, 2007; *Hyer et al.*, 2007b].

[57] To determine whether there is a relationship between the magnitude of ΔCO observed at the observatory and the initial injection height, we divided fire-affected periods into two groups: high-CO events, characterized by ΔCO > 60 ppbv (three events total), and moderate-CO events, with ΔCO < 30 ppbv (a group of six events). We compared the ratios of modeled to observed CO enhancements (CO$_{BB_T}$/ΔCO) for these groups, using both simulations (300 m and 7.5 km injection height). Average CO$_{BB_T}$/ΔCO for high-CO events dropped from 0.8 (for the 7.5 km simulations) to 0.4 (for the 300 m simulations), while no change was observed for moderate-CO events (with the average CO$_{BB_T}$/ΔCO of 0.6 for both runs). These results imply that high-CO events at the Pico Mountain observatory resulted from large, intense fires that injected emissions well above the boundary layer. Injection of emissions at higher altitude likely led to a shorter travel time and, possibly, to less dilution of CO during transport.

3.5. NO$_{xBB_T}$/CO$_{BB_T}$ Versus ΔNO$_y$/ΔCO

[58] The tracers mixing ratios, NO$_{xBB_T}$ and CO$_{BB_T}$, have uncertainties resulting from both transport modeling errors and errors associated with the emissions estimation. In the remainder of this paper, we analyze enhancement ratios, observed and simulated, in order to minimize the effects of uncertainties in the transport simulations, and focus on the consistency of the observations with estimated emission ratios.

[59] The tracer ratios (NO$_{xBB_T}$/CO$_{BB_T}$) are presented in Figure 4a (black asterisks) by day of year. These simulated enhancement ratios are somewhat higher in the early summer season (8.5×10^{-3} mol mol^{-1} in June–July) compared to the late summer season (7.3×10^{-3} mol mol^{-1} from August to early September) as a result of the increased
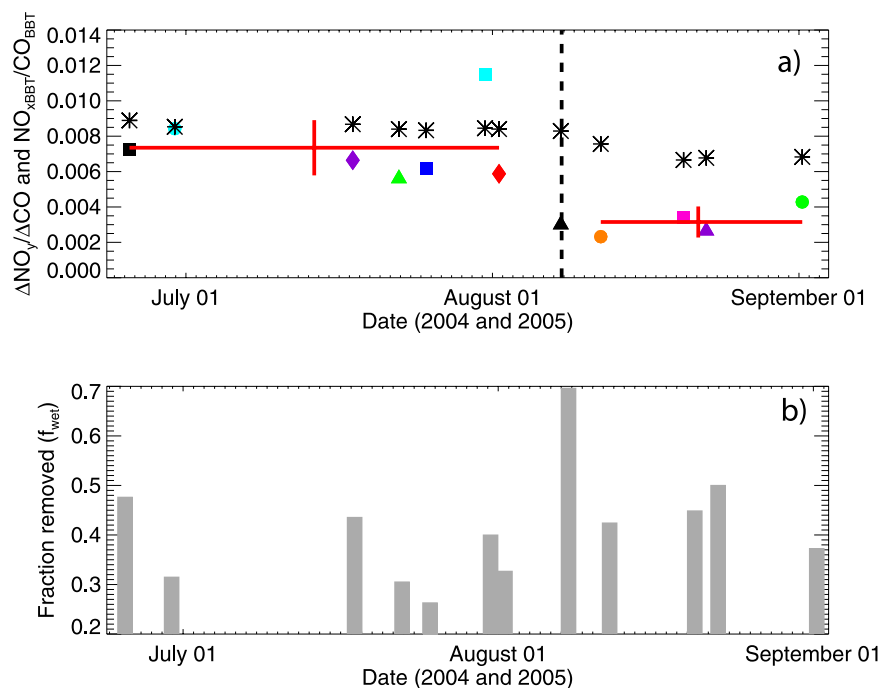
Figure 4. (a) Measured and modeled enhancement ratios during the fire-affected periods at the Pico Mountain observatory, in units of $\times 10^{-3}$ mol mol^{-1}. Shown are NO$_{xBB_T}$/CO$_{BB_T}$, simulated without wet removal (asterisks), and measured ΔNO$_y$/ΔCO enhancement ratios (coded as shown in Figure 3). Solid lines represent early and late summer averages of ΔNO$_y$/ΔCO $\pm$ 2 standard error of the mean. (b) f_{WET}, an indicator of wet-removed fraction.

smoldering combustion simulated in August, and are very similar (within 5%) to the spatially averaged NO$_x$/CO emission ratios, since the species are treated as conserved tracers. Measured NO$_y$ enhancement ratios (ΔNO$_y$/ΔCO) are also shown in Figure 4a (solid symbols). While the measured ratios follow a similar pattern, they exhibit more scatter and a larger decline in August than NO$_{xBB_T}$/CO$_{BB_T}$.

[60] To assess the consistency of the observations with the model, we computed the ratio of observed to modeled enhancement ratios (ΔNO$_y$/ΔCO)/(NO$_{xBB_T}$/CO$_{BB_T}$). If CO were treated as conserved and the modeled emissions are correct, the deviation of this ratio from unity would indicate the degree of NO$_y$ loss between emission and sampling. The mean ratio between observed and modeled enhancement ratios, (ΔNO$_y$/ΔCO)/(NO$_{xBB_T}$/CO$_{BB_T}$), dropped from 0.90 in June−July to 0.50 in August. If the emissions were correct, this would indicate NO$_y$ loss of about 10% in June−July and about 50% in August. Although the magnitude of NO$_y$ loss after emission is poorly characterized, it is very likely that the loss is significantly greater than 10%, as discussed in section 3.3. This implies that the modeled NO$_x$/CO emission ratio is an underestimate, at least in the early season, and therefore that the NO$_x$ emission factors are too low, the CO emission factors are too high, or the ratio of flaming to smoldering is too low in the early season.

[61] The increased scatter in the measurements, relative to the simulated NO$_{xBB_T}$/CO$_{BB_T}$, may be due to fire-to-fire variability in emissions and injection height not captured by the model, and/or varying degrees of NO$_y$ removal during transport. The impact of wet removal is analyzed further in

the next section, followed by a discussion of the seasonal ΔNO$_y$/ΔCO decline.

3.6. Impact of Removal on ΔNO$_y$/ΔCO

[62] To test whether the observed scatter in ΔNO$_y$/ΔCO is a result of varying degrees of removal of nitric acid from the fire plumes during their multiday transport to the observatory, we used f_{WET}. Figure 4b shows f_{WET} by event as an indicator of potential wet removal. The correlation between f_{WET} and ΔNO$_y$/ΔCO was low ($r = -0.38$). On the basis of this, we conclude that most of the scatter in ΔNO$_y$/ΔCO apparent in Figure 4a was not the result of varying NO$_y$ removal, but was most likely the result of a fire-to-fire variability in emissions and/or initial NO$_y$ export efficiency during lofting into the FT near or above the fires.

3.7. NO$_x$/CO Seasonal Trend

[63] The decline in ΔNO$_y$/ΔCO observed during the late fire season is consistent with expectations based on an increase in the relative importance of smoldering combustion, as discussed in section 2.2. To quantify the magnitude of this decline, we first divided the fire plumes into early and late summer subsets. These subsets were divided using the late season start day used by BWEM (1 August), and taking into account that the shortest transport time from fire source regions to the observatory is 7 days, as modeled by FLEXPART. Therefore, all measurements made at the Pico Mountain observatory prior to 8 August were included into the early summer subset, and the measurements made after that date constitute the late summer subset. Although this division is somewhat arbitrary, it is consistent with the

decline in the observed ratios. One event was located on the border between these subsets, on 8 August. This event also had the largest wet removal value (f_{WET} = 0.7). Although ΔNO$_y$/ΔCO during this event was similar to that in the late summer events, this event was excluded from further analysis.

[64] The mean ΔNO$_y$/ΔCO ratios for the early and late summer subsets are plotted on Figure 4 using solid lines. We employed a nonparametric Wilcoxon Sum-rank test and a two-sample t test to test for differences between two means. The early and late summer means are significantly different (α = 0.01), with significantly higher values in the early summer subset (7.3 $\times$ 10^{-3} mol mol^{-1}) relative to the late summer subset (2.8 $\times$ 10^{-3} mol mol^{-1}).

4. Conclusions

[65] Using ΔNO$_y$/ΔCO enhancement ratios observed in aged fire plumes, this work presents the first evidence of a seasonal trend in NO$_x$/CO emission ratios from boreal fires, with higher values in early summer and lower values in late summer. This trend is consistent with our understanding of the seasonal progression of boreal fire activity, in particular an increase in the amount of fuel consumed by smoldering combustion later in the growing season due to deeper burning of the drier surface layer fuels. This change in burning properties affects the relative proportions of species released from fires, leading to enhanced emissions of compounds with larger emission factors for smoldering combustion and reduced emissions of flaming combustion products. A major growth in overall fuel consumption in the late summer is also expected, due to higher levels of fuel consumption in surface organic layers. These changes are not accounted for in prior inventories of boreal forest fire NO$_x$ emissions, but they can result in considerable differences in estimated emissions and, hence, are expected to significantly affect the results of modeled ozone production rates.

[66] Tracer transport simulations of CO and NO$_x$ emissions from fires were in reasonably good agreement with the measurements. The NO$_x$ emission factors used in this work represent the best information currently available in the published literature. However, comparison of simulated NO$_{xBB_T}$/CO$_{BB_T}$ with ΔNO$_y$/ΔCO in the aged fire plumes suggests that NO$_{xBB_T}$/CO$_{BB_T}$ ratios were underestimated in the early season. This indicates that either NO$_x$ emission factors were underestimated, CO emission factors were overestimated, the model's ratio of flaming to smoldering combustion in the early season was too low, or a combination of these errors was present. The seasonal trend in this disagreement favors the third cause, which would imply that the magnitude of the seasonal drop in emission ratios from boreal fires might be even larger than simulated. The inability of the model to simulate the observed drop indicates that further research on the depth of ground layer burning in the boreal regions and on boreal fire NO$_x$ emission factors is needed.

[67] High ΔNO$_y$/ΔCO enhancement ratios measured at the Pico Mountain observatory and the poor correlation of these ratios with f_{WET}, an indicator of wet removal, implies efficient lofting and transport of NO$_y$ from boreal fires.

[68] There was a better agreement between measurements and simulated mixing ratios when emissions were released up to 7.5 km compared to the case when the maximum injection height of 300 m was used, implying the importance of pyroconvection in the boreal region. The presumed injection height was most important for the events with the highest ΔCO, pointing to large intense fires as their source.

[69] There is evidence of an increase in area burned in boreal regions in recent years, and further increases are predicted [*Flannigan et al.*, 2005; *Kasischke and Turetsky*, 2006; *Soja et al.*, 2007]. In addition, deeper seasonal thawing of permafrost and increased depth of burning are predicted [*Kasischke and Turetsky*, 2006]. The results presented here indicate that this would further shift the relative amounts of species emitted during flaming and smoldering combustion and increase total emissions with implications for atmospheric impacts.

References

Andreae, M. O. (2004), Assessment of global emissions from vegetation fires, *Int. For. Fire News*, *31*, 112–121.

Andreae, M. O., and P. Merlet (2001), Emission of trace gases and aerosols from biomass burning, *Global Biogeochem. Cycles*, *15*, 955–966.

Ayers, G. (2001), Comment on regression analysis of air quality data, *Atmos. Environ.*, *35*, 2423–2425.

Colarco, P. R., M. R. Schoeberl, B. G. Doddridge, L. T. Marufu, O. Torres, and E. J. Welton (2004), Transport of smoke from Canadian forest fires to the surface near Washington, D. C.: Injection height, entrainment, and optical properties, *J. Geophys. Res.*, *109*, D06203, doi:10.1029/2003JD004248.

Cook, P. A., et al. (2007), Forest fire plumes over the North Atlantic: p-TOMCAT model simulations with aircraft and satellite measurements from the ITOP/ICARTT campaign, *J. Geophys. Res.*, *112*, D10S43, doi:10.1029/2006JD007563.

Damoah, R., et al. (2006), A case study of pyro-convection using transport model and remote sensing data, *Atmos. Chem. Phys.*, *6*, 173–185.

DeBell, L., R. W. Talbot, J. E. Dibb, J. W. Munger, E. V. Fischer, and S. E. Frolking (2004), A major regional air pollution event in the northeastern United States caused by extensive forest fires in Quebec, Canada, *J. Geophys. Res.*, *109*, D19305, doi:10.1029/2004JD004840.

de Gouw, J. A. (2006), Volatile organic compounds composition of merged and aged forest fire plumes from Alaska and western Canada, *J. Geophys. Res.*, *111*, D10303, doi:10.1029/2005JD006175.

Draper, N. R., and H. Smith (1998), *Applied Regression Analysis*, John Wiley, Hoboken, N. J.

Duncan, B. N., R. V. Martin, A. C. Staudt, R. Yevich, and J. A. Logan (2003), Interannual and seasonal variability of biomass burning emissions constrained by satellite observations, *J. Geophys. Res.*, *108*(D2), 4100, doi:10.1029/2002JD002378.

Edwards, D. P., et al. (2004), Observations of carbon monoxide and aerosols from the TERRA satellite: Northern Hemisphere variability, *J. Geophys. Res.*, *109*, D24202, doi:10.1029/2004JD004727.

European Centre for Medium-Range Weather Forecasts (2005), Users guide to ECMWF products 4.0, *Tech. Rep. Meteorol. Bull. M3.2*, Reading, U. K.

Flannigan, M. D., K. A. Logan, B. D. Amiro, W. R. Skinner, and B. Stocks (2005), Future area burned in Canada, *Clim. Change*, *72*, 1–16.

French, N. H. F., P. Goovaerts, and E. S. Kasischke (2004), Uncertainty in estimating carbon emissions from boreal forest fires, *J. Geophys. Res.*, *109*, D14S08, doi:10.1029/2003JD003635.

French, N., E. Kasischke, M. R. Turetsky, W. de Groot, R. Honrath, and R. Ottmar (2007), Carbon, trace gas, and particulate emissions from wildfires in the boreal regions of North America, paper presented at 16th International Emission Inventory Conference, Environ. Prot. Agency, Raleigh, N. C.

Fromm, M. D., and R. Servranckx (2003), Transport of forest fire smoke above the tropopause by supercell convection, *Geophys. Res. Lett.*, 30(10), 1542, doi:10.1029/2002GL016820.

Fromm, M., R. Bevilacqua, R. Servranckx, J. Rosen, J. P. Thayer, J. Herman, and D. Larko (2005), Pyro-cumulonimbus injection of smoke to the stratosphere: Observations and impact of a super blowup in northwestern Canada on 3–4 August 1998, *J. Geophys. Res.*, 110, D08205, doi:10.1029/2004JD005350.

Generoso, S., I. Bey, J.-L. Attie, and F.-M. Breon (2007), A satellite-and model-based assessment of the 2003 Russian fires: Impact on the Arctic region, *J. Geophys. Res.*, 112, D15302, doi:10.1029/2006JD008344.

Goode, J. G., R. J. Yokelson, D. E. Ward, R. A. Susott, R. E. Babbitt, M. A. Davies, and W. M. Hao (2000), Measurements of excess O$_3$, CO, CH$_4$, C$_2$H$_4$, C$_2$H$_2$, HCN, NO, NH$_3$, HCOOH, CH$_3$COOH, HCHO, and CH$_3$OH in 1997 Alaskan biomass burning plumes by airborne Fourier transform infrared spectroscopy (AFTIR), *J. Geophys. Res.*, 105(D17), 22,147–22,166, doi:10.1029/2000JD900287.

Honrath, R. E., R. C. Owen, M. Val Martín, J. S. Reid, K. Lapina, P. Fialho, M. P. Dziobak, J. Kleissl, and D. L. Westphal (2004), Regional and hemispheric impacts of anthropogenic and biomass burning emissions on summertime CO and O$_3$ in the North Atlantic lower free troposphere, *J. Geophys. Res.*, 109, D24310, doi:10.1029/2004JD005147.

Hudman, R. C. (2007), Surface and lightning sources of nitrogen oxides over the United States: Magnitudes, chemical evolution, and outflow, *J. Geophys. Res.*, D12S05, doi:10.1029/2006JD007912.

Hyer, E. J., E. S. Kasischke, and D. J. Allen (2007a), Effects of source temporal resolution on transport simulations of boreal fire emissions, *J. Geophys. Res.*, 112, D01302, doi:10.1029/2006JD007234.

Hyer, E. J., D. J. Allen, and E. S. Kasischke (2007b), Examining injection properties of boreal forest fires using surface and satellite measurements of CO transport, *J. Geophys. Res.*, 112, D18307, doi:10.1029/2006JD008232.

Jacob, D. J., et al. (1992), Summertime photochemistry of the troposphere at high northern latitudes, *J. Geophys. Res.*, 97, 16,421–16,431.

Jost, H.-J., et al. (2004), In-situ observations of mid-latitude forest fire plumes deep in the stratosphere, *Geophys. Res. Lett.*, 31, L11101, doi:10.1029/2003GL019253.

Kasischke, E. S., and L. P. Bruhwiller (2002), Emissions of carbon dioxide, carbon monoxide, and methane from boreal forest fires in 1998, *J. Geophys. Res.*, 108(D1), 8146, doi:10.1029/2001JD000461.

Kasischke, E. S., and J. F. Johnstone (2005), Variation in postfire organic layer thickness in a black spruce forest complex in interior Alaska and its effects on soil temperature and moisture, *Can. J. For. Res.*, 35, 2164–2177.

Kasischke, E. S., and M. R. Turetsky (2006), Recent changes in the fire regime across the North American boreal region—Spatial and temporal patterns of burning across Canada and Alaska, *Geophys. Res. Lett.*, 33, L09703, doi:10.1029/2006GL025677.

Kasischke, E. S., D. Williams, and D. Barry (2002), Analysis of the patterns of large fires in the boreal forest region of Alaska, *Int. J. Wildland Fire*, 11(2), 131–144.

Kasischke, E. S., E. J. Hyer, P. C. Novelli, L. P. Bruhwiler, N. H. F. French, A. I. Sukhinin, J. H. Hewson, and B. J. Stocks (2005), Influences of boreal fire emissions on Northern Hemisphere atmospheric carbon and carbon monoxide, *Global Biogeochem. Cycles*, 19, GB1012, doi:10.1029/2004GB002300.

Kleissl, J., R. Honrath, M. Dziobak, D. Tanner, M. Val Martn, R. Owen, and D. Helmig (2007), The occurrence of upslope flows at the Pico mountaintop observatory: A case study of orographic flows on small, volcanic island, *J. Geophys. Res.*, 112, D10S35, doi:10.1029/2006JD007565.

Lapina, K., R. E. Honrath, R. C. Owen, M. Val Martín, and G. Pfister (2006), Evidence of significant large-scale impacts of boreal fires on ozone levels in the midlatitude Northern Hemisphere free troposphere, *Geophys. Res. Lett.*, 33, L10815, doi:10.1029/2006GL025878.

Leung, F.-Y., J. A. Logan, R. Park, E. Hyer, E. Kasischke, D. Streets, and L. Yurganov (2007), Impacts of biomass burning in the boreal forests on tropospheric chemistry and the sensitivity of model results to injection height, *J. Geophys. Res.*, 112, D10313, doi:10.1029/2006JD008132.

Li, Q., D. J. Jacob, J. W. Munger, R. M. Yantosca, and D. D. Parrish (2004), Export of NO$_y$ from the North American boundary layer: Reconciling aircraft observations and global model budgets, *J. Geophys. Res.*, 109, D02313, doi:10.1029/2003JD004086.

Lobert, J. M., D. H. Scharffe, W. M. Hao, T. A. Kuhlbusch, R. Seuwen, P. Warneck, and P. J. Crutzen (1991), Experimental evaluation of biomass burning emissions: Nitrogen and carbon containing compounds, in *Global Biomass Burning: Atmospheric, Climatic, and Biospheric Implications*, edited by J. S. Levine, chap. 36, pp. 289–307, MIT Press, Cambridge, Mass.

Luderer, G., J. Trentmann, T. Winterrath, C. Textor, M. Herzog, H. F. Graf, and M. O. Andreae (2006), Modeling of biomass smoke injection into the lower stratosphere by a large forest fire (Part II): Sensitivity studies, *Atmos. Chem. Phys.*, 6, 5261–5277.

Mason, S. A., R. J. Field, R. J. Yokelson, M. A. Kochivar, M. R. Tinsley, D. E. Ward, and W. M. Hao (2001), Complex effects arising in smoke plume simulations due to inclusion of direct emissions of oxygenated organic species from biomass combustion, *J. Geophys. Res.*, 106, 12,527–12,539.

Mauzerall, D. L., et al. (1998), Photochemistry in biomass burning plumes and implications for tropospheric ozone over the tropical South Atlantic, *J. Geophys. Res.*, 103, 8401–8423.

Mazzoni, D., J. A. Logan, D. Diner, R. Kahn, L. Tong, and Q. Li (2007), A data-mining approach to associating misr smoke plume heights with modis fire measurements, *Remote Sens. Environ.*, 107, 138–148.

McKeen, S. A., G. Wotawa, D. D. Parrish, J. S. Holloway, M. P. Buhr, F. C. Fehsenfeld, and J. F. Meagher (2002), Ozone production from Canadian wildfires during June and July of 1995, *J. Geophys. Res.*, 107(D14), 4192, doi:10.1029/2001JD000697.

Miyanishi, K. (2001), Duff consumption, in *Forest Fires: Behavior and Ecological Effects*, edited by E. A. Johnson and K. Miyanishi, pp. 437–475, Academic, San Diego, Calif.

Morris, G. A., et al. (2006), Alaskan and Canadian forest fires exacerbate ozone pollution over Houston, Texas, on 19 and 20 July 2004, *J. Geophys. Res.*, 111, D24S03, doi:10.1029/2006JD007090.

Nance, J. D., P. V. Hobbs, L. F. Radke, and D. E. Ward (1993), Airborne measurements of gases and particles from an Alaskan wildfire, *J. Geophys. Res.*, 98, 14,873–14,882, doi:10.1029/93JD01196.

Novelli, P. C., K. A. Masarie, P. M. Lang, B. D. Hall, R. C. Myers, and J. W. Elkins (2003), Reanalysis of tropospheric CO trends: Effects of the 1997–1998 wildfires, *J. Geophys. Res.*, 108(D15), 4464, doi:10.1029/2002JD003031.

Olivier, J., and J. Berdowski (2001), Global emissions sources and sinks, in *The Climate System*, vol. 33–78, edited by J. Berdowski, R. R. Guicherit, and B. Heij, A. A. Balkema, Brookfield, Vt.

Owen, R., O. Cooper, A. Stohl, and R. Honrath (2006), An analysis of the mechanisms of transport of North American emissions to the central North Atlantic, *J. Geophys. Res.*, 111, D23S58, doi:10.1029/2006JD007062.

Parrish, D. D., et al. (2004), Fraction and composition of NO$_y$ transported in air masses lofted from the North American boundary layer, *J. Geophys. Res.*, 109, D09302, doi:10.1029/2003JD004226.

Pfister, G., P. G. Hess, K. Emmons, J.-F. Lamarque, C. Wiedinmyer, D. P. Edwards, G. Pétron, J. C. Gille, and G. W. Sachse (2005), Quantifying CO emissions from the 2004 Alaskan wildfires using MOPITT CO data, *Geophys. Res. Lett.*, 32, L11809, doi:10.1029/2005GL022995.

Pfister, G., et al. (2006), Ozone production from the 2004 North American boreal fires, *J. Geophys. Res.*, 111, D24S07, doi:10.1029/2006JD007695.

Real, E., et al. (2007), Processes influencing ozone levels in Alaskan forest fire plumes during long-range transport over the North Atlantic, *J. Geophys. Res.*, 112, D10S41, doi:10.1029/2006JD007576.

Roy, B., G. A. Pouliot, A. Gilliland, T. Pierce, S. Howard, P. V. Bhave, and W. Benjey (2007), Refining fire emissions for air quality modeling with remotely sensed fire counts: A wildfire case study, *Atmos. Environ.*, 41, 655–665, doi:10.1016/j.atmosenv.2006.08.037.

Sapkota, A., et al. (2005), Impact of the 2002 Canadian forest fires on particulate matter air quality in Baltimore city, *Environ. Sci. Technol.*, 39, 24–32, doi:10.1021/es035311z.

Seibert, P., and A. Frank (2004), Source-receptor matric calculation with a Lagrangian particle disperion model in backward mode, *Atmos. Chem. Phys.*, 4, 51–63.

Singh, H. B., et al. (2007), Reactive nitrogen distribution and partitioning in the North American troposphere and lowermost stratosphere, *J. Geophys. Res.*, 112, D12S04, doi:10.1029/2006JD007664.

Soja, A. J., et al. (2007), Climate-induced boreal forest change: Predictions versus current observations, *Global and Planet. Change*, 56, 274–296, doi:10.1016/j.gloplacha.2006.07.028.

Stohl, A., S. Eckhardt, C. Forster, P. James, N. Spichtinger, and P. Seibert (2002), A replacement for simple back trajectory calculations in the interpretation of atmospheric trace substance measurements, *Atmos. Environ.*, 36, 4635–4648.

Stohl, A., C. Forster, A. Frank, P. Seibert, and G. Wotawa (2005), Technical note: The Lagrangian particle dispersion model FLEXPART version 6.2, *Atmos. Chem. Phys.*, 5, 2461–2474, sref:1680-7324/acp/2005-5-2461.

Stohl, A., et al. (2006), Pan-arctic enhancements of light absorbing aerosol concentrations due to North American boreal forest fires during summer 2004, *J. Geophys. Res.*, 111, D22214, doi:10.1029/2006JD007216.

Trentmann, J., G. Luderer, T. Winterrath, M. D. Fromm, R. Servranckx, C. Textor, M. Herzog, H. F. Graf, and M. O. Andreae (2006), Modeling of biomass smoke injection into the lower stratosphere by a large forest fire (Part I): Reference simulation, *Atmos. Chem. Phys.*, *6*, 5247–5260.

Turetsky, M. R., B. D. Amiro, E. Bosch, and J. S. Bhatti (2004), Historical burn area in western canadian peatlands and its relationship to fire weather indices, *Global Biogeochem. Cycles*, *18*, GB4014, doi:10.1029/2004GB002222.

Turquety, S., et al. (2007), Inventory of boreal fire emissions for North America in 2004: The importance of peat burning and pyro-convective injection, *J. Geophys. Res.*, *112*, D12S03, doi:10.1029/2006JD007281.

Val Martín, M., R. Honrath, R. C. Owen, G. Pfister, P. Fialho, and F. Barata (2006), Significant enhancements of nitrogen oxides, ozone and aerosol black carbon in the North Atlantic lower free troposphere resulting from North American boreal wildfires, *J. Geophys. Res.*, *111*, D23S60, doi:10.1029/2006JD007530.

Wofsy, S. C., et al. (1992), Atmospheric chemistry in the arctic and sub-arctic: Influence of natural fires, industrial emissions, and stratospheric inputs, *J. Geophys. Res.*, *97*, 16,731–16,746.

Wofsy, S. C., S.-M. Fan, D. R. Blake, J. D. Bradshaw, S. T. Sandholm, H. B. Singh, G. W. Sachse, and R. C. Harriss (1994), Factors influencing atmospheric composition over subarctic North America during summer, *J. Geophys. Res.*, *99*, 1887–1897.

Wotawa, G., P. C. Novelli, M. Trainer, and C. Granier (2001), Inter-annual variability of summertime CO concentrations in the Northern Hemisphere explained by boreal forest fires in North America and Russia, *Geophys. Res. Lett.*, *28*, 4575–4578.

Yokelson, R. J., D. W. T. Griffith, and D. E. Ward (1996), Open-path Fourier transform infrared studies of large-scale laboratory biomass fire, *J. Geophys. Res.*, *101*, 21,067–21,080.

Yokelson, R. J., R. Susott, D. E. Ward, J. Reardon, and D. W. T. Griffith (1997), Emissions from smoldering combustion of biomass measured by open-path Fourier transform infrared spectroscopy, *J. Geophys. Res.*, *102*, 18,865–18,878, doi:10.1029/97JD00852.

————————————

P. Fialho, Climate, Meteorology and Global Change Center, Group of Chemistry and Physics of the Atmosphere, University of the Azores, PT9701-851 Terra Chã, Portugal.

R. E. Honrath, K. Lapina, and R. C. Owen, Department of Civil and Environmental Engineering, Michigan Technological University, Houghton, MI 49931, USA. (klapina@mtu.edu)

E. J. Hyer, Marine Meteorology Division, Naval Research Laboratory, Monterey, CA 93943, USA.

M. Val Martín, Division of Engineering and Applied Sciences, Harvard University, Cambridge, MA 02138, USA.